Loss of TDAG51 Results in Mature-Onset Obesity, Hepatic Steatosis, and Insulin Resistance by Regulating Lipogenesis

Sana Basseri,[1,2] Šárka Lhoták,[2] Morgan D. Fullerton,[3] Rengasamy Palanivel,[3] Hua Jiang,[4] Edward G. Lynn,[1,2] Rebecca J. Ford,[3] Kenneth N. Maclean,[4] Gregory R. Steinberg,[3] and Richard C. Austin[1,2]

Regulation of energy metabolism is critical for the prevention of obesity, diabetes, and hepatic steatosis. Here, we report an important role for the pleckstrin homology–related domain family member, T-cell death–associated gene 51 (*TDAG51*), in the regulation of energy metabolism. TDAG51 expression was examined during adipocyte differentiation. Adipogenic potential of preadipocytes with knockdown or absence of *TDAG51* was assessed. Weight gain, insulin sensitivity, metabolic rate, and liver lipid content were also compared between TDAG51-deficient (*TDAG51*$^{-/-}$) and wild-type mice. In addition to its relatively high expression in liver, TDAG51 was also present in white adipose tissue (WAT). TDAG51 was downregulated during adipogenesis, and *TDAG51*$^{-/-}$ preadipocytes exhibited greater lipogenic potential. *TDAG51*$^{-/-}$ mice fed a chow diet exhibited greater body and WAT mass, had reduced energy expenditure, displayed mature-onset insulin resistance (IR), and were predisposed to hepatic steatosis. *TDAG51*$^{-/-}$ mice had increased hepatic triglycerides and SREBP-1 target gene expression. Furthermore, TDAG51 expression was inversely correlated with fatty liver in multiple mouse models of hepatic steatosis. Taken together, our findings suggest that TDAG51 is involved in energy homeostasis at least in part by regulating lipogenesis in liver and WAT, and hence, may constitute a novel therapeutic target for the treatment of obesity and IR. ***Diabetes* 62:158–169, 2013**

With a dramatic rise in the prevalence of obesity and type 2 diabetes worldwide, there is an urgent need to better understand the genes involved in the metabolic processes underlying these conditions. Obesity results from an increase in white adipose tissue (WAT) mass, which occurs as a result of two processes, adipocyte hypertrophy and hyperplasia. The former process indicates an increase in adipocyte size, and the latter is the result of an increase in mature adipocyte number through preadipocyte recruitment and adipocyte differentiation (1,2). The transcription factors peroxisome proliferator–activated receptor γ (PPARγ) (3,4) and CCAAT/enhancer–binding protein-α (C/EBPα) (5–7) play a crucial role during adipogenesis. In the later stages of terminal differentiation, proteins such as adipocyte-specific fatty acid–binding protein (aP2), adiponectin, and leptin are expressed (8). A fine balance between adipocyte hypertrophy and adipogenesis exists to prevent the formation of dysfunctional adipose tissue, since large cells are more likely to be insulin resistant (9,10) and therefore can influence adipose tissue metabolism. Despite significant progress over the last few years, additional genes and factors that influence adipogenesis, adipose tissue metabolism, and ultimately energy homeostasis still remain to be uncovered.

A recent microarray analysis of differentiating 3T3-L1 preadipocytes found T-cell death associated gene 51 (*TDAG51*), among other genes, to be induced within the first 8 h of adipogenesis (11) and was categorized in the same gene cluster as *C/EBPβ* and *C/EBPδ*, early adipogenic genes crucial for initiating the adipogenic gene expression cascade (12). Given the importance of the first 24 h in determining preadipocyte cell fate (13,14), this finding suggests that *TDAG51* may be a novel candidate gene involved in adipogenesis. TDAG51 is a member of the pleckstrin homology (PH)–like domain family (human homolog PHLDA1) (15) and was first demonstrated to be induced upon T-cell activation–mediated apoptosis in culture (16). However, in contrast to these in vitro findings, TDAG51-deficient (*TDAG51*$^{-/-}$) mice displayed no apparent defects in T-cell apoptosis, number, or function (17). In addition to its PH-like domain, TDAG51 possesses distinct COOH-terminal proline-glutamine and proline-histidine repeats (18), which may be involved in its pro-apoptotic function in some cell types (19). TDAG51 has been suggested to play a role in tumorigenesis (20,21), and we have previously shown its expression in atherosclerotic lesions from hyperhomocysteinemic mice (22), although the precise physiological role of TDAG51 is not well understood. To date, the role of TDAG51 in adipogenesis and energy metabolism has not been examined.

We evaluated the protein expression pattern of TDAG51 in several tissues of wild-type (WT) C57BL/6 mice, which indicated that in addition to liver, which expresses the highest levels of TDAG51, WAT also expresses TDAG51. Here we report that TDAG51 expression was modulated during adipogenesis and that *TDAG51*$^{-/-}$ preadipocytes exhibited greater lipid accumulation under adipogenic conditions as compared with WT cells. *TDAG51*$^{-/-}$ mice displayed an age-related increase in whole-body adiposity and an overall metabolic profile resembling the metabolic syndrome. Furthermore, TDAG51 expression was inversely

From the [1]Division of Nephrology, Department of Medicine, McMaster University, Hamilton, Ontario, Canada; the [2]Hamilton Centre for Kidney Research, St. Joseph's Healthcare Hamilton, Hamilton, Ontario, Canada; the [3]Division of Endocrinology and Metabolism, Department of Medicine, McMaster University, Hamilton, Ontario, Canada; and the [4]Department of Pediatrics, University of Colorado School of Medicine, Aurora, Colorado.
Corresponding author: Richard C. Austin, austinr@taari.ca.
Received 29 February 2012 and accepted 17 July 2012.
DOI: 10.2337/db12-0256
This article contains Supplementary Data online at http://diabetes.diabetesjournals.org/lookup/suppl/doi:10.2337/db12-0256/-/DC1.

correlated with fatty liver in several mouse models of hepatic steatosis. These findings suggest a previously unknown function for TDAG51 in promoting negative energy balance by regulating adipocyte and hepatic lipogenesis, thereby favoring energy expenditure.

RESEARCH DESIGN AND METHODS

Western blotting and antibodies. Cells and tissues were homogenized in 4× SDS lysis buffer, and protein lysates were subjected to immunoblotting as previously described (23). Antibodies were used to detect the following proteins: TDAG51, SREBP-1 (H160 for detection of precursor p125 and K10 for detection of mature p68), C/EBPα, PPARα (Santa Cruz Biotechnology), Akt, pS473-Akt, Scd-1, fatty acid synthase (FAS), phosphoserine insulin receptor substrate 1 (phosphoserine IRS1), aP2, PPARγ, perilipin, glyceraldehyde-3-phosphate dehydrogenase (GAPDH) (Cell Signaling), IRS1, phosphotyrosine IRS1 (Invitrogen), and β-actin (Sigma).

Cell culture. Mouse 3T3-L1 cells were cultured, differentiated, and stained with Oil Red O as previously described (23). Pooled protein extracts were obtained from isolated human preadipocytes and their corresponding differentiated adipocytes from four lean female subjects (Zenbio).

mRNA quantification by real-time PCR. Total RNA was isolated using the RNeasy kit (Qiagen) according to the manufacturer's protocol. Using a High-Capacity cDNA Reverse Transcription Kit (Applied Biosystems), total RNA was reverse transcribed to obtain cDNA. Quantitative real time-PCR (qRT-PCR) was performed using Fast SYBR Green PCR Master Mix (Applied Biosystems) in the AB7900 HT Fast Real-Time PCR System. For a list of primer sequences see Supplementary Table 1. Data analysis was performed using the ΔΔC(T) method and normalized to 18S, unless otherwise indicated.

Isolation and culturing of primary cells. Primary preadipocytes were cultured by isolating the stromal-vascular fraction from mouse WAT. In brief, WAT was minced, collagenase (Sigma) digested, and centrifuged to separate the stromal-vascular fraction from the mature adipocyte fraction. The pelleted cells were then plated and induced to differentiate in Dulbecco's modified Eagle's medium/F12 containing 2% FBS, 1 μg/mL insulin, 250 nmol/L dexamethasone, 0.5 mmol/L isobutylmethylxanthine, 60 μmol/L indomethacin, and 2.5 μmol/L rosiglitazone. Cells were stained with Oil Red O as previously described (23), or protein lysates were collected for Western blotting. Primary hepatocytes isolated from the liver were plated on collagen-coated six-well plates (BD) and allowed to attach for 2–3 h in Williams' medium E (Invitrogen), after which medium was replaced with Williams' medium E containing 10% FBS. Isolated hepatocytes were incubated overnight at 37°C and the experiments were performed the following day.

Mice. *TDAG51*$^{-/-}$ mice were generated previously (17) and back-crossed onto the C57BL/6 background for at least nine generations and genotyped as described in the Supplementary Data. C57BL/6 or *TDAG51*$^{-/-}$ mice were maintained under 12-h light-dark cycles with unlimited access to standard rodent chow and water. At 8 weeks of age, male WT or *TDAG51*$^{-/-}$ mice ($n = 8$) were either continued on the regular chow diet or placed on a high-fat diet (42% of kcal from fat, TD.88137; Harlan Teklad). At 28 weeks of age, mice were fasted for 14 h before they were killed by cervical dislocation under anesthesia. Blood was drawn from the heart, and tissues were immediately collected for histology or biochemical assessment. Only male mice were used in this study. Unless stated otherwise, only chow diet–fed mice were examined. All protocols for animal use and euthanasia were approved by the McMaster University Animal Research Ethics Board.

Computed tomography and positron emission tomography. WT and *TDAG51*$^{-/-}$ mice were fasted overnight and given an intravenous injection of 2-(^{18}F) fluoro-2-deoxyglucose (2-FDG). The mice were kept under heat lamps for 30 min, anesthetized using isoflurane, and scanned on a small animal positron emission tomography (PET) scanner for visualization of glucose uptake. The mice were placed in a single-photon emission computed tomography (SPECT)/CT scanner for determination of body fat content (24).

Biochemical analyses. Plasma adiponectin (R&D Systems), leptin (Linco), and insulin (Chemicon) concentrations were measured using mouse ELISA kits. Plasma glucose, triglycerides (TGs), cholesterol esters, and free fatty acids (FFAs) were measured using colorimetric assays from Wako Diagnostics. Plasma thiobarbituric acid reactive substances (TBARS) assay was carried out using an OXI-TEK TBARS Kit (Alexis Biochemicals), and plasma alanine aminotransferase (ALT) levels were analyzed using a kit (ThermoDMA).

Cytometric inflammatory bead array. Plasma cytokines were measured using a bead cytometric array (BD) according to the manufacturer's protocol.

Metabolic studies. For glucose tolerance tests (GTTs), mice were fasted overnight and given an intraperitoneal injection of glucose (1.5 mg/g body weight). For insulin tolerance tests (ITTs), mice were fasted for 6 h and intraperitoneally injected with 0.75 units/kg of insulin. Blood was collected from the tail vein, and glucose concentrations were measured using a hand-held glucometer. For in vivo insulin signaling experiments, tissues were collected 15 min after an intraperitoneal injection of insulin (0.75 units/kg) in fasted mice as previously described (25). Metabolic studies using indirect calorimetry were performed using the Columbus Laboratory Animal Monitoring System (CLAMS) as described previously (26). Core body temperature was determined in the CLAMS after subcutaneous implantation, under isoflurane anesthesia, of minimiter probes (Respironics, Inc.) in the dorsal subscapular region.

Transmission electron microscopy. Interscapular brown adipose tissue (BAT) was excised, cut into 2-mm^3 pieces, and immersed in 2% glutaraldehyde in cacodylate buffer. Tissues were processed using standard protocols and embedded in Spurr resin. Ultrathin sections were stained with uranyl acetate and lead citrate and observed under a JEOL 200CX TEMSCAN microscope.

Hepatic TG content and VLDL-TG secretion. Approximately equivalent weights of frozen liver tissue from mice were homogenized in PBS, and TGs were extracted using the Folch extraction method as previously described (27). Hepatic VLDL-TG secretion was measured as previously described (28). In brief, fasted 8-week-old mice were injected intraperitoneally with 1 g/kg poloxamer-407 dissolved in saline, and blood samples were collected for serum TG measurements at various time points.

Hepatocyte de novo lipogenesis and palmitate oxidation. For determination of de novo lipogenesis, hepatocytes were incubated with media containing sodium acetate (5 mmol/L) and ^{3}H-acetate (1 μCi/mL; Perkin Elmer) for 1 or 4 h in the presence or absence of 10 nmol/L insulin. Cells were washed twice with PBS, and lipids were extracted by the method of Bligh and Dyer (29). Neutral lipids were quantified as previously described (30). Lipid bands were visualized and scraped into counting vials for measuring radioactivity. Palmitate oxidation was determined as described previously (31). In brief, sodium palmitate (0.5 mmol/L) and ^{14}C-palmitate (0.5 μCi/mL; Perkin Elmer) were allowed to conjugate to 2% BSA for 2–3 h and then incubated with primary hepatocytes for 4 h, in the presence or absence of 10 nmol/L insulin. Radiolabeled CO_2 was liberated by adding an equal volume of 1 mol/L acetic acid and trapped by the addition of benzethonium hydroxide (1 mol/L) over 90 min. The tube containing trapped $^{14}CO_2$ was placed in a scintillation vial and counted.

Statistical analysis. Data are expressed as the mean ± SEM unless otherwise indicated. Statistical analyses were performed using unpaired, two-tailed Student t test, and significance was defined as $P < 0.05$.

RESULTS

TDAG51 is expressed in preadipocytes and is downregulated during adipogenesis. TDAG51 protein expression was examined in various tissues from adult C57BL/6 mice. In addition to the liver and lung, which have abundant TDAG51 levels at the mRNA and protein level (15,17), WAT also expressed TDAG51 protein (Fig. 1*A*). Previous microarray analysis during adipogenesis indicated that *TDAG51* mRNA expression is modulated in early adipogenesis (11). Therefore, we carried out qRT-PCR analysis, which confirmed that *TDAG51* mRNA was significantly induced in the first 2 h of adipogenesis followed by a sharp decline back to baseline expression (Fig. 1*B*). We next sought to evaluate the expression profile of TDAG51 at the protein level during adipocyte differentiation. TDAG51 protein expression was induced in the first 4 days post-stimulation, followed by a gradual decline after day 4, and diminished expression by day 14 of differentiation, when the vast majority of cells had accumulated large lipid droplets, as shown by Oil Red O staining (Fig. 1*C*, *top*). In addition, TDAG51 expression showed an inverse correlation with PPARγ expression during adipogenesis (Fig. 1*C*).

In support of the findings in 3T3-L1 cells, an inverse correlation between TDAG51 and PPARγ expression and/or adipogenesis was also observed in mouse embryonic fibroblasts induced to differentiate into adipocytes (Fig. *1D*). We next examined protein extracts from pooled human preadipocytes and their corresponding differentiated mature adipocytes, which also showed disappearance of TDAG51 in mature adipocytes (Fig. 1*E*). These findings indicate that TDAG51 is downregulated in differentiated lipid-laden adipocytes, suggesting that TDAG51 may play an important role in adipogenesis.

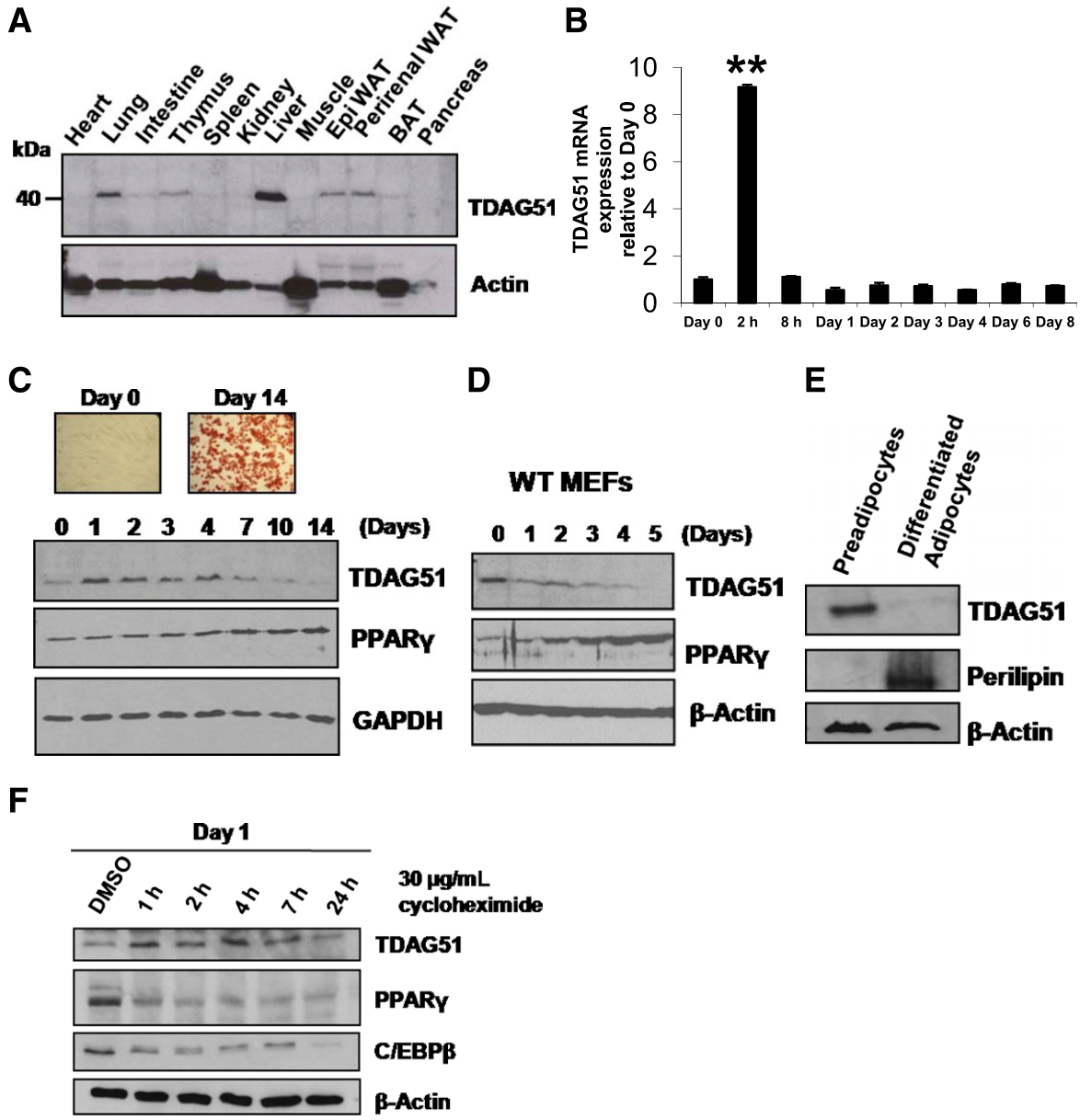

FIG. 1. TDAG51 is expressed in preadipocytes and is downregulated during adipogenesis. *A*: Western blotting for TDAG51 using whole-tissue lysates from WT C57BL/6 mice. *B*: qRT-PCR for *TDAG51* mRNA expression in 3T3-L1 preadipocytes during differentiation. Data represent the mean ± SD. **$P < 0.01$ vs. day 0 cells. *C*: 3T3-L1 cells were induced to differentiate for 14 days and stained with Oil Red O to detect neutral lipids (*top*). Total lysates were assessed for PPARγ, TDAG51, and glyceraldehyde-3-phosphate dehydrogenase (GAPDH; loading control) by immunoblotting (*bottom*). *D*: Mouse embryonic fibroblasts (MEFs) isolated from WT C57BL/6 mice were induced to differentiate (at passage 5), and protein extracts were collected and subjected to immunoblotting. β-Actin was used as a loading control. *E*: TDAG51, perilipin (positive control for mature adipocytes), and β-actin protein expression in human preadipocyte and corresponding mature adipocyte protein extracts (pooled from four subjects). *F*: 3T3-L1 cells on day 1 of differentiation were treated with 30 μg/mL cycloheximide, and protein lysates were collected at the indicated time points. TDAG51, PPARγ, C/EBPβ, and β-actin expression were assessed through immunoblotting. (A high-quality color representation of this figure is available in the online issue.)

To reconcile the temporal difference in the expression of TDAG51 mRNA and protein during adipogenesis, 3T3-L1 cells were treated with cycloheximide to block protein translation. As shown in Fig. 1*F*, relative to other proteins that are crucial for adipogenesis, such as PPARγ and C/EBPβ, TDAG51 protein is considerably more stable.

Absence of TDAG51 enhances lipid accumulation by altering early adipogenic gene expression during adipogenesis. In order to examine the role of TDAG51 in adipogenesis, primary stromal-vascular cells (SVCs) were isolated from WT and *TDAG51*$^{-/-}$ WAT and induced to differentiate. *TDAG51*$^{-/-}$ SVCs exhibited earlier and/or greater expression of adipogenic markers such as PPARγ2, aP2, FAS, perilipin, and C/EBPα on day 2 (Fig. 2*A*). By day 5, most of these adipogenic markers reached similar levels in WT and *TDAG51*$^{-/-}$ SVCs. However, despite the plateau in expression of these adipogenic markers, *TDAG51*$^{-/-}$ SVCs exhibited increased lipid accumulation, as determined by Oil Red O staining (Fig. 2*B*), and enhanced adiponectin secretion, a marker of mature adipocytes (Fig. 2*C*).

To complement these findings, both silencing/short interfering (si)RNA and short hairpin (sh)RNA targeting mouse *TDAG51* were used to knockdown TDAG51

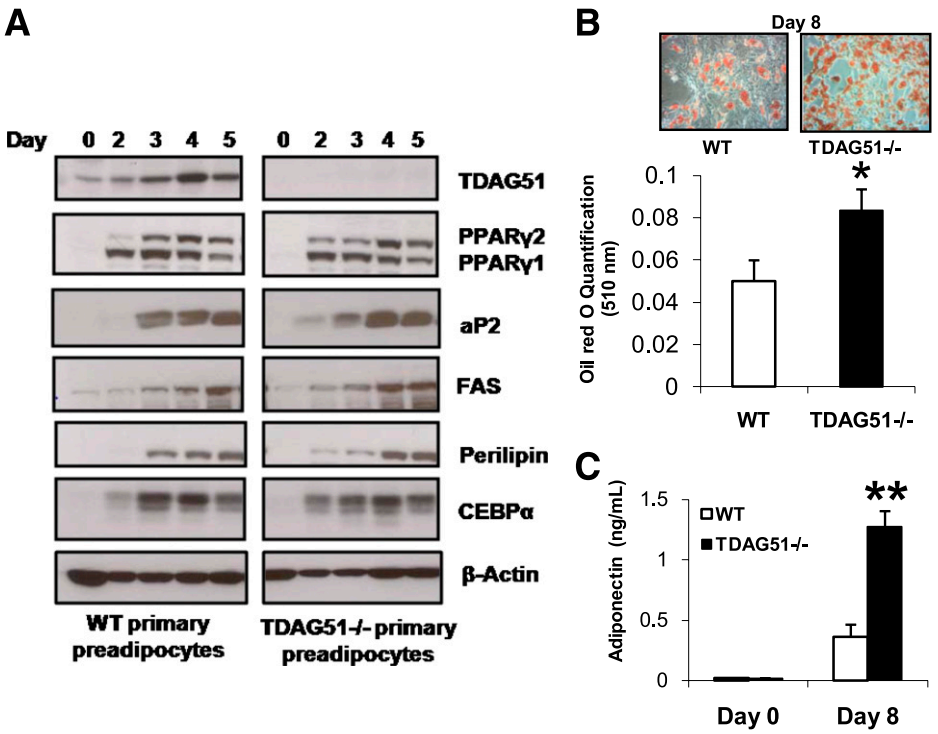

FIG. 2. Absence of TDAG51 enhances lipid accumulation in adipocytes. *A*: Immunoblotting for adipogenic markers on day 0, 2, 3, 4, and 5 of WT or *TDAG51*$^{-/-}$ primary preadipocyte differentiation. *B*: Preadipocytes on day 8 were stained with Oil Red O and representative images were taken (*top*). The staining was quantified (*bottom*) (n = 3). *C*: Adiponectin secretion from primary preadipocytes (n = 5). Data are expressed as the mean ± SD. *P < 0.05 and **P < 0.01 vs. WT on the same day of differentiation. (A high-quality color representation of this figure is available in the online issue.)

expression in 3T3-L1 cells. Similar to *TDAG51*$^{-/-}$ SVCs, siTDAG51-transfected cells had significantly greater lipid accumulation compared with siControl-transfected cells (Supplementary Fig. 1*A* and *B*). An shTDAG51 construct was used, leading to a stable 30% knockdown in TDAG51 mRNA expression (Supplementary Fig. 1*C*). Even this modest decrease in mRNA expression led to a striking decrease in TDAG51 protein (Supplementary Fig. 1*D*) and resulted in significantly greater adiponectin secretion from shTDAG51 cells on day 3 (Supplementary Fig. 1*E*). Expression of *C/EBPδ* and *C/EBPβ* mRNA was higher within the first 8 h of differentiation but dropped off more quickly, and similarly mRNA expression of preadipocyte factor-1 (*Pref-1*) declined more quickly in shTDAG51 cells on day 1 as compared with shControl cells (Supplementary Fig. 1*F*). Analysis of late markers of adipogenesis, such as expression of *PPARγ*, *aP2*, and *C/EBPα* mRNA, indicated that they were expressed earlier (day 2) and to a greater extent in shTDAG51 cells (Supplementary Fig. 1*G*).

***TDAG51*$^{-/-}$ mice develop increased adiposity due to reduced basal energy expenditure.** To study the effect of loss of TDAG51 on weight regulation in vivo, 8-week-old chow diet–fed male *TDAG51*$^{-/-}$ mice were monitored over 20 weeks and compared with age- and sex-matched heterozygous *TDAG51*$^{+/-}$ and WT mice. Body weight was not significantly different between genotypes at 8 weeks of age (Fig. 3*A* and Supplementary Fig. 2). However, over time, in comparison with WT mice, *TDAG51*$^{-/-}$ mice exhibited a significant increase in body weight (Fig. 3*A*), which was not observed for *TDAG51*$^{+/-}$ mice (Supplementary Fig. 2). There was no significant difference in tissue weights (Supplementary Fig. 3*A* and *B*) except for epididymal WAT (eWAT), where a significant increase was observed in *TDAG51*$^{-/-}$ mice (Fig. 3*B*). CT scans in 28-week-old mice showed that *TDAG51*$^{-/-}$ mice have a fivefold increase in total body WAT (Fig. 3*C*), with fat deposition in both the visceral and subcutaneous depots (Fig. 3*C*, *top*). A significant increase in adiposity was also observed in the bone marrow of *TDAG51*$^{-/-}$ mice (Supplementary Fig. 4*A* and *B*). Histological examination of the eWAT revealed that *TDAG51*$^{-/-}$ adipocytes were significantly enlarged compared with WT controls (Fig. 3*D*). In support of enhanced adipogenic and lipogenic potential observed in cultured preadipocytes (Fig. 2*A*–*C*), mRNA expression of several adipogenic genes (*aP2*, *PPARγ*, and *C/EBPβ*) was significantly increased in WAT from *TDAG51*$^{-/-}$ mice (Fig. 3*E*). These findings demonstrate that absence of TDAG51 enhances adipocyte lipid accumulation, leading to WAT expansion and increased body mass in *TDAG51*$^{-/-}$ mice.

Consistent with increased adiposity, *TDAG51*$^{-/-}$ mice had increased levels of systemic oxidative stress (TBARS) (Table 1), reaching levels similar to age-matched diet-induced obese mice (Supplementary Table 2), as well as increased plasma leptin and reduced adiponectin concentrations, compared with WT mice (Table 1). Plasma inflammatory markers (tumor necrosis factor-α [TNF-α], monocyte chemoattractant protein-1 [MCP-1], and IL12p70) tended to be higher in *TDAG51*$^{-/-}$ mice, but did not reach statistical significance (Supplementary Fig. 5*A*). Furthermore, staining of eWAT sections to detect macrophages revealed an increase in the number of crown-like structures in comparison with WT mice (Supplementary Fig. 5*B*). These findings are consistent with the notion that increased adiposity leads to adipose macrophage infiltration.

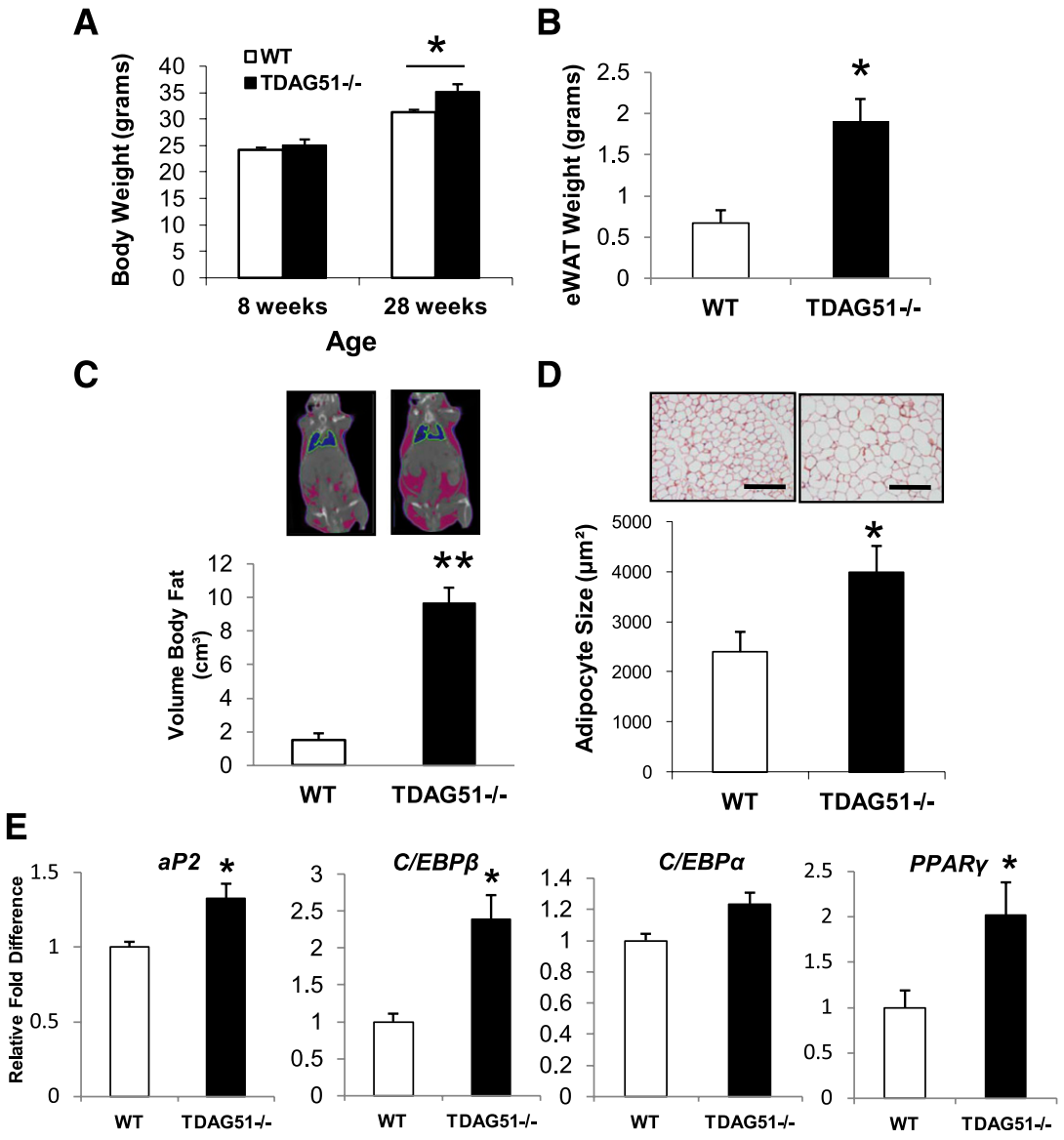

FIG. 3. *TDAG51*$^{-/-}$ **mice develop increased adiposity with enlarged adipocytes.** ***A*****: Body weights at 8 and 28 weeks of age in male WT or** *TDAG51*$^{-/-}$ **mice (*n* = 7–8).** ***B*****: eWAT weight at 28 weeks of age (*n* = 7).** ***C*****: CT scans in 28-week-old WT and** *TDAG51*$^{-/-}$ **mice. Representative images are shown, with pink areas depicting the quantified WAT areas (*n* = 5, **$P < 0.001$).** ***D*****: Perilipin-stained, paraffin-embedded eWAT is shown in the top panel (bar, 250 µm). Adipocyte size is in µm² (*n* = 7).** ***E*****: Adipogenic gene expression in WAT from 8-week-old mice, normalized to cyclophilin (*n* = 6). Data are expressed as the mean ± SEM. *$P < 0.05$ vs. WT. (A high-quality color representation of this figure is available in the online issue.)**

We next examined metabolic parameters using indirect calorimetry. Food consumption in WT and *TDAG51*$^{-/-}$ mice was not significantly different (Fig. 4*A*), and although there was a trend toward lower locomotor activity in *TDAG51*$^{-/-}$ mice, the difference did not reach statistical significance (Fig. 4*B*). However, *TDAG51*$^{-/-}$ mice exhibited a decrease in metabolic rate as indicated by a significant reduction in oxygen consumption (V_{O_2}) during both day and night hours (Fig. 4*C*). Core body temperature was also lower in *TDAG51*$^{-/-}$ mice during the night, which corresponded with their lower V_{O_2} (Fig. 4*D*).

We explored whether changes in BAT, an important regulator of thermogenesis in mice, could explain the difference in energy expenditure. Interscapular BAT from WT

TABLE 1
Plasma metabolic parameters in fasted 28-week-old WT and *TDAG51*$^{-/-}$ mice on chow diet

Plasma	ALT (units/L)	TBARS (µmol/L)	Chol-E (mg/dL)	FFA (mmol/L)	TG (mg/dL)	Adiponectin (µg/mL)	Leptin (ng/mL)
WT	33.3 ± 3.5	0.15 ± 0.1	92.3 ± 5.7	0.65 ± 0.03	48.5 ± 5.4	11.9 ± 0.8	1.9 ± 0.5
TDAG51$^{-/-}$	32.3 ± 3.8	3.75 ± 1.3*	94.8 ± 2.6	0.81 ± 0.06*	49.0 ± 2.2	6.3 ± 0.6**	14.7 ± 2.6**

Data shown in the table represent means ± SEM. ALT (*n* = 6–7); TBARS (*n* = 6–7); cholesterol-E (Chol-E) (*n* = 7–8); FFA (*n* = 7–8); TGs (*n* = 7–8); adiponectin (*n* = 7–8); leptin (*n* = 7–8). *$P < 0.05$, between WT and *TDAG51*$^{-/-}$. **$P < 0.01$, between WT and *TDAG51*$^{-/-}$.

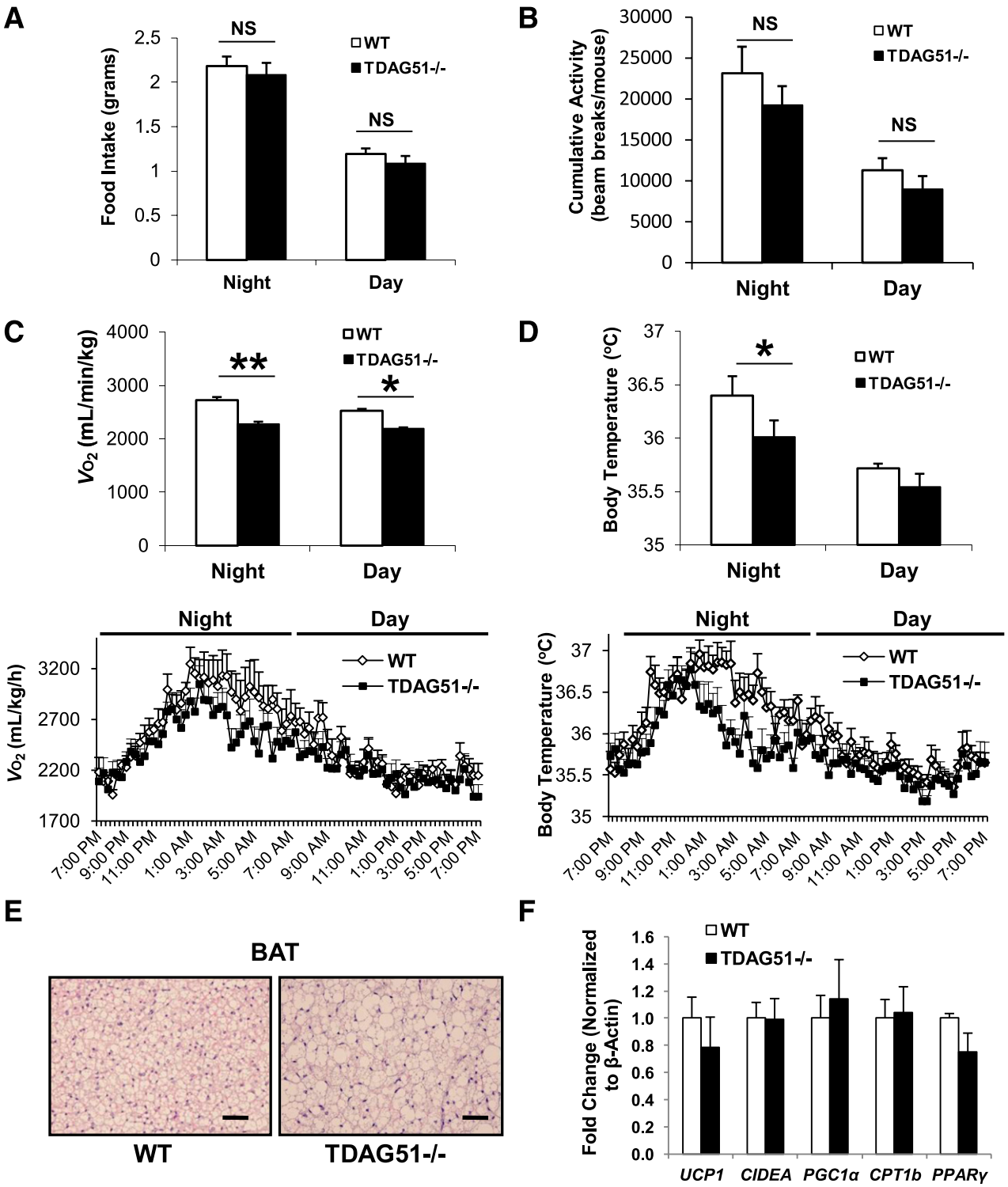

FIG. 4. Energy expenditure is reduced in *TDAG51*$^{-/-}$ mice. *A*: Food intake at 20 weeks of age (n = 7). *B*: Total locomotor activity in 20-week-old mice during day and night hours (n = 7). NS, not significant. Vo_2 (oxygen uptake) (*C*) and core body temperature (*D*) in 20-week-old mice (n = 7). *E*: Hematoxylin-eosin–stained BAT from 28-week-old mice (Bar, 50 μm). *F*: Gene expression analysis of thermogenic and mitochondrial genes in BAT (n = 6–7). Data are expressed as the mean ± SEM. *P < 0.05 and **P < 0.01 vs. WT. (A high-quality color representation of this figure is available in the online issue.)

and *TDAG51*$^{-/-}$ mice was examined to assess cell morphology, and we found an overall increase in lipid droplet size in BAT from *TDAG51*$^{-/-}$ mice (Fig. 4*E*). We next examined expression of thermogenic and mitochondrial genes in BAT from WT and *TDAG51*$^{-/-}$ mice. No significant differences were found in the expression of *UCP1*, *CIDEA*, *PGC1α*, *CPT1b*, or *PPARγ*, and we did not detect any differences in the expression of components of the electron transport chain (Supplementary Fig. 6*A*). Furthermore, no overall difference in UCP-1 immunostaining of BAT paraffin sections was observed between genotypes (Supplementary Fig. 6*B*). To assess mitochondrial morphology and

size, BAT was further examined using transmission electron microscopy; however, no striking differences in mitochondria shape, size, or cristae were observed between genotypes (Supplementary Fig. 6*C*). Given that TDAG51 expression is ~90% lower in BAT compared with WAT of WT mice (Supplementary Fig. 6*D*), it is possible that BAT function in *TDAG51*$^{-/-}$ mice would not be directly affected by the absence of TDAG51. These findings suggest an increase in ectopic lipid deposition in BAT; however, BAT function does not appear to be significantly affected.

***TDAG51*$^{-/-}$ mice develop age-associated insulin resistance.** Fasting plasma glucose and insulin levels were significantly elevated in *TDAG51*$^{-/-}$ mice at 28 weeks of age (Fig. 5*A* and *B*). In young 8-week-old WT and *TDAG51*$^{-/-}$ mice, an age where whole-body, liver, and WAT weights were indistinguishable (Fig. 3*A* and Supplementary Fig. 7*A*), GTTs and ITTs revealed no differences between genotypes (Supplementary Fig. 7*B* and *C*). However, at 28 weeks of age, when *TDAG51*$^{-/-}$ mice exhibited a significant increase in WAT and body weight, *TDAG51*$^{-/-}$ mice were also significantly more glucose intolerant (Fig. 5*C*) and insulin resistant (Fig. 5*D*) compared with WT mice. The efficiency of glucose uptake in various tissues was examined using PET scanning, which revealed a significant decrease in glucose uptake in skeletal muscles and WAT of *TDAG51*$^{-/-}$ mice (Fig. 5*E*). WAT from *TDAG51*$^{-/-}$ mice also showed decreased insulin receptor signaling, as indicated by reduced tyrosine (Y608) phosphorylation of IRS-1 and increased phosphorylation on serine (S612), which inhibits insulin receptor signaling (Fig. 5*F*). However, at least within this time interval, insulin-stimulated Akt phosphorylation and SREBP-1 activation were similar in WAT from WT and *TDAG51*$^{-/-}$ mice. Consistent with the presence of increased adiposity, decreased glucose disposal, and insulin resistance (IR), plasma FFAs were also significantly elevated in *TDAG51*$^{-/-}$ mice (Table 1).

To investigate the cause of hyperinsulinemia and IR in *TDAG51*$^{-/-}$ mice, pancreatic islets were histologically assessed using insulin and glucagon staining. No discernible differences in islet size or shape were observed between genotypes (Fig. 5*G*). Overall, these findings demonstrate that *TDAG51*$^{-/-}$ mice display an age-related impairment in insulin sensitivity that is likely related to increased adiposity in these mice.

TDAG51 expression is inversely correlated with fatty liver, and *TDAG51*$^{-/-}$ mice exhibit hepatic steatosis due to enhanced lipogenesis. Given the high levels of TDAG51 expression in the liver, we sought to determine if TDAG51 expression was altered in fatty livers by examining three mouse models of nonalcoholic fatty liver disease. Dietary, genetic, and chemically induced steatosis were all highly correlated with reduced TDAG51 protein expression (Fig. 6*A*). Interestingly, absence of TDAG51 increased hepatic lipid accumulation and steatosis in 28-week-old mice on chow diet, as determined by histological staining and biochemical measurement of liver TG (Fig. 6*B* and *C*), a phenotype that was exacerbated in *TDAG51*$^{-/-}$ mice fed a high-fat diet for 20 weeks (Fig. 6*B*). Given that significant metabolic differences existed between genotypes on a standard chow diet, only chow diet–fed mice were further examined. To rule out the possibility that loss of TDAG51 resulted in hepatic TG accumulation due to impaired hepatic VLDL-TG secretion, serum TG concentrations were measured over the course of 4 h after injection of poloxamer-407, an inhibitor of lipoprotein lipase. There were no significant differences in the rate of hepatic TG secretion (Fig. 6*D*).

TDAG51$^{-/-}$ livers showed increased staining for proteins covalently adducted with 4-hydroxynonenal, a marker of lipid peroxidation (Fig. 6*E*), and an increased number of granulomas indicative of inflammation (Fig. 6*F*), both of which are consistent with greater steatosis. However, there were no signs of hepatocellular injury as measured by plasma ALT (Table 1), and hepatic cholesterol content was not affected (data not shown). In agreement with increased hepatic TG in *TDAG51*$^{-/-}$ livers, there was a marked increase in insulin-stimulated SREBP-1 activation, a master regulator of hepatic lipogenesis (32–34), as indicated by reduced expression of the precursor form of SREBP-1 (p125) and enhanced expression of the mature form (p68) (Fig. 6*G*), which was not affected under basal fasted conditions (Supplementary Fig. 8*A*). Insulin-injected *TDAG51*$^{-/-}$ livers also had reduced serine 473 phosphorylation of Akt, suggestive of hepatic IR (Fig. 6*G*). Expression of lipogenic enzymes and SREBP-1 target genes, FAS and stearoyl-CoA desaturase-1 (Scd-1), were induced in livers from *TDAG51*$^{-/-}$ mice under basal fasting conditions (Fig. 6*H*). Furthermore, preliminary microarray gene expression analysis of liver from chow diet–fed WT and *TDAG51*$^{-/-}$ mice (K.N.M., R.C.A., unpublished data) revealed an increase in >10 SREBP target genes in *TDAG51*$^{-/-}$ livers (Supplementary Table 3).

To determine whether these results were secondary to the insulin-resistant phenotype or intrinsic to the loss of TDAG51, primary hepatocytes from 6-week-old WT and *TDAG51*$^{-/-}$ mice, which displayed no differences in body weight or metabolic phenotype, were examined. *TDAG51*$^{-/-}$ hepatocytes responded normally to insulin (Supplementary Fig. 8*B*) but had enhanced basal and insulin-stimulated lipogenesis (rate of newly synthesized fatty acid incorporation into TG) (Fig. 7*A*). Palmitate oxidation, on the other hand, was not different between genotypes when examined basally or upon insulin stimulation in primary hepatocytes (Fig. 7*B*). Furthermore, levels of PPARα, a transcription factor involved in fatty acid catabolism, was not affected by the absence of TDAG51 in liver tissue (Supplementary Fig. 8*A*). Consistent with enhanced de novo lipogenesis, primary hepatocytes from *TDAG51*$^{-/-}$ mice expressed higher mRNA levels of the SREBP-1c target genes glucokinase (*GK*) and acetyl CoA carboxylase 1 (*ACC1*) (Fig. 7*C*). These results in cultured hepatocytes are in full agreement with our findings in livers from *TDAG51*$^{-/-}$ mice, suggesting that deletion of *TDAG51* promotes lipogenesis at least in part through increased SREBP-1 activation and its downstream target gene expression.

DISCUSSION

Dysregulation of the pathways involved in adipogenesis, lipid metabolism, and energy homeostasis can lead to the development of obesity, hepatic steatosis, diabetes, and dyslipidemia. Here, we present novel evidence that TDAG51 plays a significant role in the regulation of energy and lipid metabolism. First, the findings of this study show for the first time that TDAG51 is expressed in WAT and that its protein expression is modulated during adipogenesis. Given that TDAG51 protein expression is minimal or absent in mature mouse and human adipocytes, TDAG51 may be a useful preadipocyte marker. Second, deletion of TDAG51 enhances lipid accumulation during adipogenesis and accelerates fatty acid/TG synthesis in

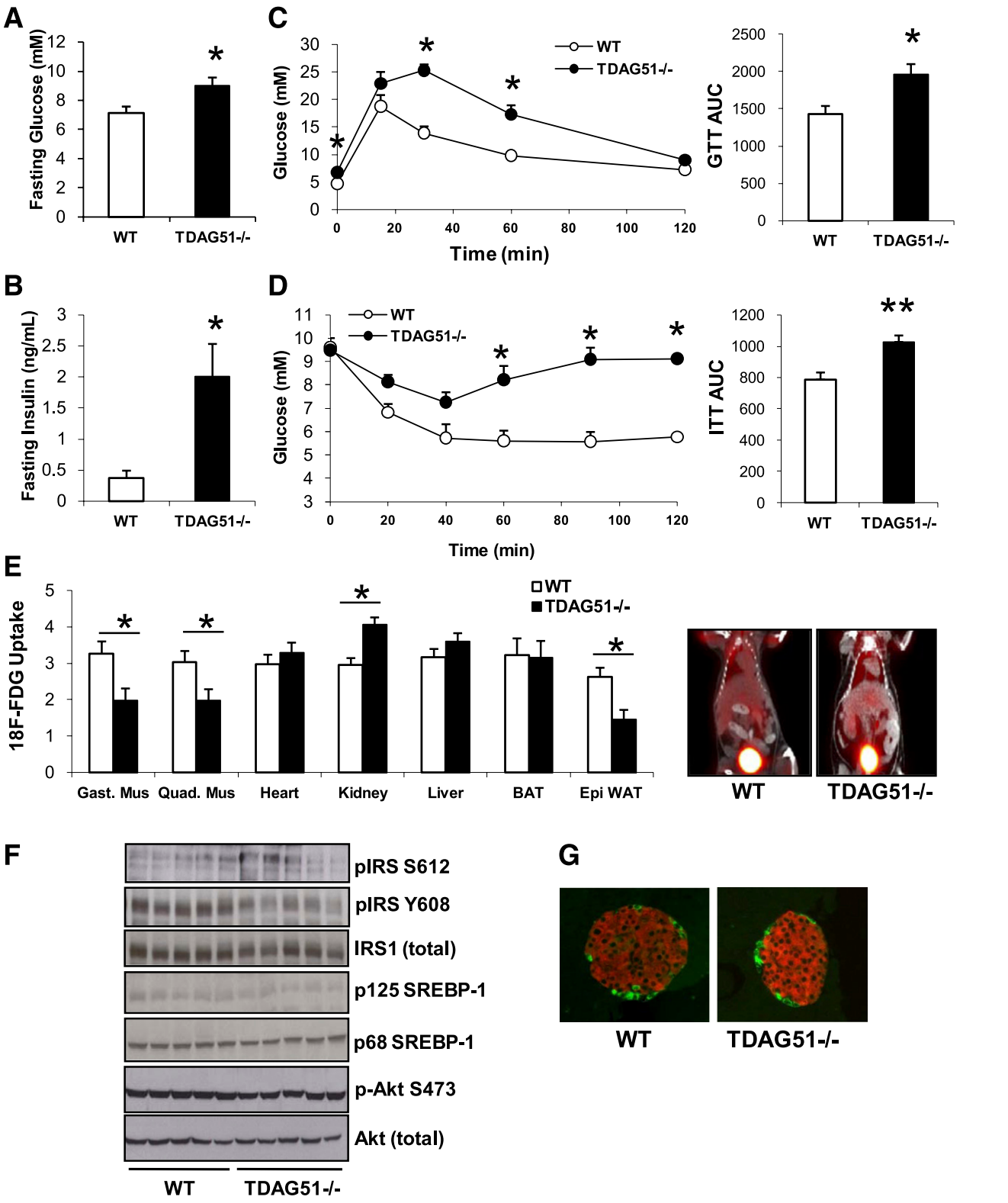

FIG. 5. *TDAG51*$^{-/-}$ **mice develop age-associated IR. Fasting glucose (*A*) and fasting insulin (*B*) concentrations in 28-week-old male mice (n = 7–8). *C*: GTT after an overnight fast and the area under the curve (AUC) in the right panel (n = 4). *D*: ITT after a 6-h fast and the AUC (*right*) (n = 6–7). *E*: Intravenous injection of 2-FDG followed by a PET scan. Quantification of 2-FDG in various tissues (n = 5). PET scan images from representative mice are shown in the right panel. *F*: Mice were injected with insulin after a 6-h fast, and eWAT was collected 15 min later for Western blotting examining insulin receptor signaling (n = 5 mice). *G*: Pancreatic islets taken at the same magnification, where red staining represents insulin and green depicts glucagon. Data are expressed as the mean ± SEM. **P* < 0.05 and ***P* < 0.01 vs. WT.**

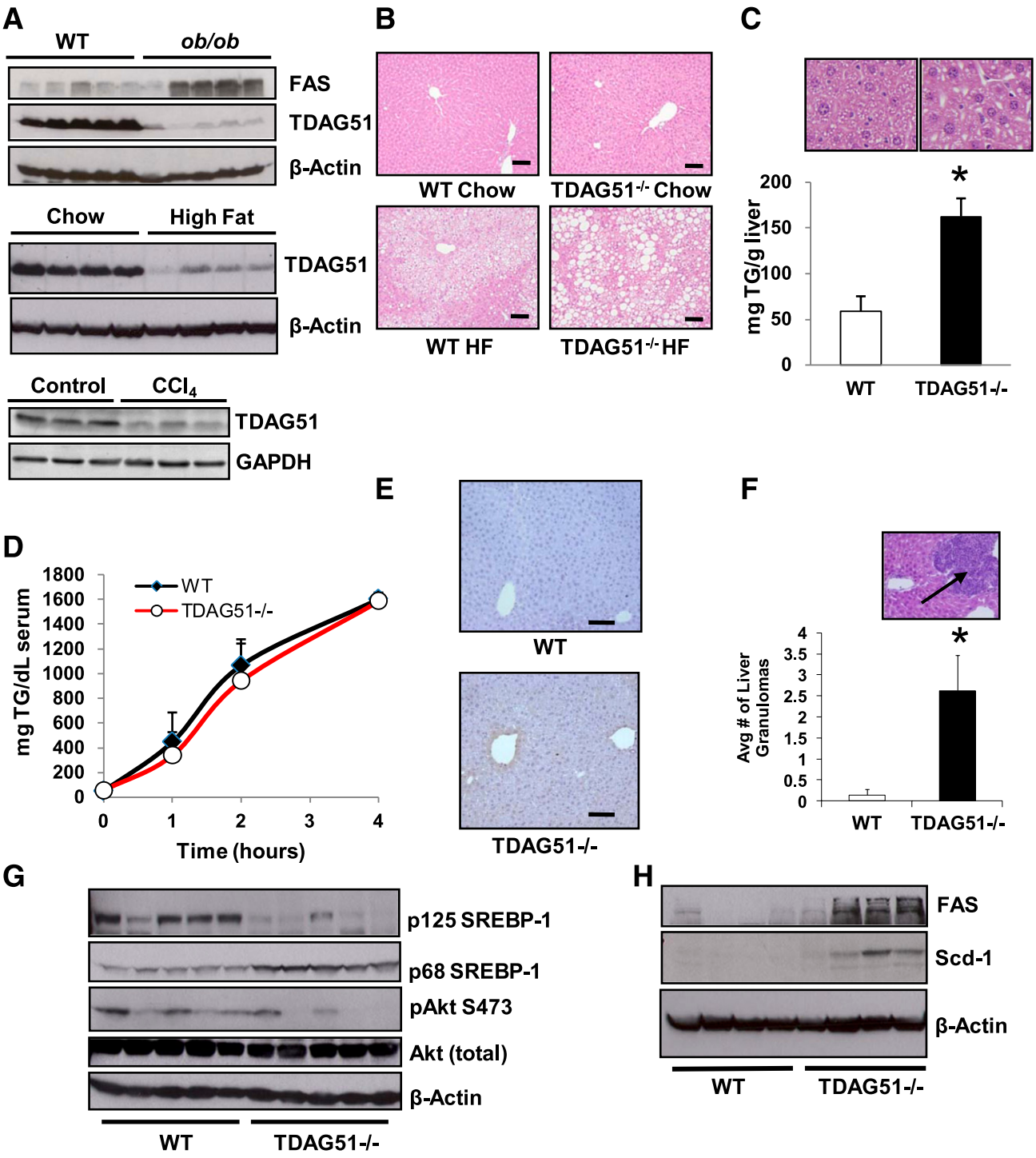

FIG. 6. TDAG51 is negatively correlated with fatty liver, and absence of TDAG51 leads to hepatic steatosis. *A*: TDAG51 expression in liver protein lysates from age-matched WT and *ob/ob* mice (*top*) ($n = 5$), chow- and high-fat diet–fed (*middle*) ($n = 4$), as well as control and carbon tetrachloride (CCl_4)–treated mice (*bottom*) ($n = 3$). *B*: Hematoxylin-eosin (H-E)–stained livers from 28-week-old WT and *TDAG51*$^{-/-}$ mice. Mice were either fed a standard chow diet (*top*) or a 42% high-fat (HF) diet for 20 weeks (*bottom*). Bar, 200 μm. *C*: Liver TG content was quantified ($n = 4$–5), and representative higher magnification images of H-E–stained livers from chow-fed mice are shown. *D*: Eight-week-old mice were injected with poloxamer-407, and serum TG was measured over 4 h. *E*: Detection of 4-hydroxynonenal in liver sections (bar, 200 μm). *F*: Quantification of inflammatory cell infiltrations (granulomas) in H-E–stained livers ($n = 5$). Arrow indicates granuloma. Avg, average. *G*: Immunoblotting for total Akt, phosphoserine 473 Akt, and SREBP-1 activation in liver lysates from mice 15 min postinsulin injection ($n = 5$). *H*: Immunoblotting of liver lysates from fasted mice ($n = 4$). Data are expressed as the mean ± SD. *$P < 0.01$ vs. WT.

primary hepatocytes. Third, the absence of TDAG51 leads to an age-associated increase in whole-body adiposity and hepatic TG accumulation, and decreases metabolic rate and insulin sensitivity in standard chow diet–fed WT mice. Notably, the phenotype observed in *TDAG51*$^{-/-}$ mice resembles several aspects of high-fat diet–fed WT mice. Finally, TDAG51 protein expression is inversely correlated with hepatic steatosis.

The age-dependent increase in adiposity, hepatic TG accumulation, and systemic IR in *TDAG51*$^{-/-}$ mice are

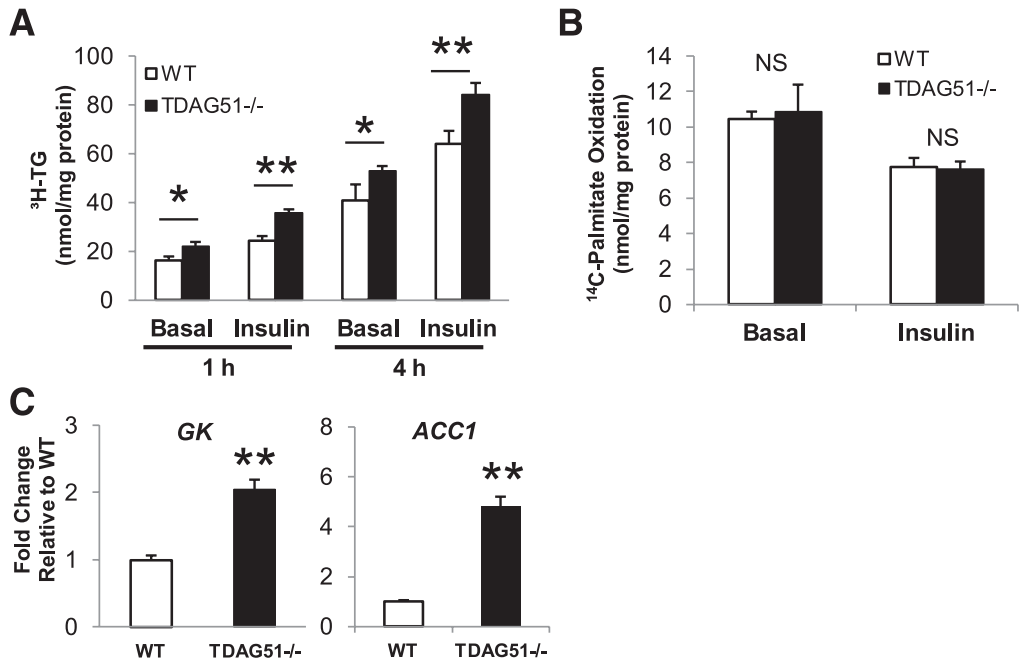

FIG. 7. ***TDAG51*$^{-/-}$ primary hepatocytes exhibit greater lipogenic potential.** ***A*: Basal and insulin-stimulated (100 nmol/L) ^{3}H-acetate incorporation into triacylglycerol (TG) in primary hepatocytes from 6-week-old mice treated with vehicle or insulin.** ***B*: ^{14}C-Palmitate oxidation in primary hepatocytes from 6-week-old mice treated with vehicle or insulin.** ***C*: qRT-PCR analysis examining mRNA expression of *GK* and *ACC1* in cultured primary hepatocytes. Data are expressed as the mean ± SEM, *n* = 3. **P* < 0.05 and ***P* < 0.01 vs. WT.**

suggestive of a chronic and cumulative effect, likely attributable to a decrease in metabolic rate and increased lipogenesis. Excessive accumulation of TG can culminate in the expansion of WAT, ectopic lipid accumulation, and eventually IR in combination with chronic inflammation and oxidative stress (35,36), which is consistent with the phenotype observed in older *TDAG51*$^{-/-}$ mice. Moreover, when cells become insulin resistant, not all pathways are blunted as lipogenic pathways remain active, a concept known as selective IR (37). The reduced Akt phosphorylation in combination with increased SREBP-1 activation seen in livers from insulin-injected *TDAG51*$^{-/-}$ mice is consistent with selective IR. The absence of TDAG51 in mice culminated in increased TG deposition in the liver. Numerous studies show a strong correlation between fatty liver and whole-body IR (38–42), suggesting that increased hepatic steatosis and selective IR in the liver of *TDAG51*$^{-/-}$ mice may be contributing to the systemic IR phenotype in these mice. Given that SREBP-1 is a master regulator of hepatic de novo lipogenesis (32–34) and an increase in SREBP-1 target gene expression was observed in *TDAG51*$^{-/-}$ livers, the absence of TDAG51 likely leads to hepatic steatosis through increased SREBP-1 activity. Consistent with this result, primary *TDAG51*$^{-/-}$ hepatocytes exhibited a significant enhancement in the rate of lipogenesis, which correlates with the strong association between TDAG51 reduction and fatty livers. Taken together, these data suggest a role for TDAG51 in the negative regulation of SREBP-mediated lipogenesis and prevention of fatty liver.

TDAG51 has several important domains, including a PH-like domain, which appears to be a likely candidate for functional significance in the context of cell signaling and metabolism. For instance, a recent study identified a novel PH domain–containing protein involved in the regulation of adipocyte insulin signaling (43). Indeed, TDAG51 was identified as a specific IGF-1 target gene in NIH-3T3 fibroblasts and was shown to mediate the effects of IGF-1 on cell survival (44). Furthermore, previous studies suggest that extracellular signal–related kinase (ERK) and p38 mitogen-activated protein kinase (p38 MAPK) signaling can modulate TDAG51 expression (44,45). However, the exact cellular mechanisms by which IGF-1, ERK, or p38 MAPK induces TDAG51 expression are unknown.

PH domains play an important role in recruiting target proteins to cell membranes through their binding interactions with phospholipids such as phosphatidylinositol (3-5)-triphosphate (PIP3) and phosphatidylinositol (4,5)-bisphosphate (PIP2) (46,47). Interestingly, TDAG51 has a high stringency PIP3-binding site in its PH-like domain, as predicted by ScanSite (48). Furthermore, the PH-like domain of TDAG51 exhibits a high degree of homology to that of phosphatidylinositol 3-kinase (PI3K) enhancer (PIKE), as predicted by the Protein Homology/Analog Y Recognition Engine (Phyre2) (49). Interestingly, PIKE has recently been implicated in playing a role in adipogenesis, WAT regulation, and insulin sensitivity, and in contrast to *TDAG51*$^{-/-}$ mice, *PIKE*$^{-/-}$ mice are protected from diet-induced weight gain and IR (50). Thus, we are currently exploring whether the PH-like domain of TDAG51 is indeed mediating its effects on the regulation of lipogenesis and whole-body energy metabolism and whether the PI3K/Akt pathway may be involved.

Collectively, the results of our study illustrate that TDAG51 plays an important role as a regulator of carbohydrate and lipid metabolism, at least in part through regulating SREBP activity, which may contribute to the phenotypes observed with the metabolic syndrome. Understanding this newly identified cellular factor in lipid metabolism and adipogenesis as well as its precise regulation under normal and pathophysiological conditions will be crucial for the development of effective treatments against diabetes and obesity.

ACKNOWLEDGMENTS

R.C.A. and G.R.S. are supported by grants from the Heart and Stroke Foundation of Ontario (NA-6024) and the Canadian Institutes of Health Research (CIHR) (MOP-111239 and MOP-67116). Financial support from St. Joseph's Healthcare Hamilton is also acknowledged. K.N.M. is supported by National Institute of Diabetes and Digestive and Kidney Diseases grant R01-DK-074487-01. S.B. is supported by a Heart and Stroke Foundation of Canada Doctoral Award. M.D.F. is a CIHR Banting Postdoctoral Fellow. G.R.S. is a Canada Research Chair in Metabolism and Obesity. R.C.A. is a Career Investigator of the Heart and Stroke Foundation of Ontario (CI-7408) and holds the Amgen Canada Research Chair in Nephrology.

No potential conflicts of interest relevant to this article were reported.

S.B. performed experiments, collected and interpreted data, and wrote the manuscript. Š.L., M.D.F., R.P., and E.G.L. performed experiments, contributed to data interpretation, and edited the manuscript. H.J. and R.J.F. assisted with experiments. K.N.M., G.R.S., and R.C.A. contributed to data interpretation and discussion and reviewed the manuscript. R.C.A. is the guarantor of this work and, as such, had full access to all the data in the study and takes responsibility for the integrity of the data and the accuracy of the data analysis.

The authors thank Dr. Y. Choi (University of Pennsylvania, Philadelphia, PA) for kindly providing the *TDAG51*$^{+/-}$ mice. The authors acknowledge the help of K. Karimi (McMaster University) with the BD cytometric bead array and are grateful to C. Saab and R. Rhem (McMaster University) for their technical assistance with the animal imaging.

REFERENCES

1. Villena JA, Viollet B, Andreelli F, Kahn A, Vaulont S, Sul HS. Induced adiposity and adipocyte hypertrophy in mice lacking the AMP-activated protein kinase-alpha2 subunit. Diabetes 2004;53:2242–2249
2. Hausman DB, DiGirolamo M, Bartness TJ, Hausman GJ, Martin RJ. The biology of white adipocyte proliferation. Obes Rev 2001;2:239–254
3. Rosen ED, Sarraf P, Troy AE, et al. PPAR gamma is required for the differentiation of adipose tissue in vivo and in vitro. Mol Cell 1999;4:611–617
4. Tontonoz P, Hu E, Spiegelman BM. Stimulation of adipogenesis in fibroblasts by PPAR gamma 2, a lipid-activated transcription factor. Cell 1994; 79:1147–1156
5. Freytag SO, Geddes TJ. Reciprocal regulation of adipogenesis by Myc and C/EBP alpha. Science 1992;256:379–382
6. Freytag SO, Paielli DL, Gilbert JD. Ectopic expression of the CCAAT/enhancer-binding protein alpha promotes the adipogenic program in a variety of mouse fibroblastic cells. Genes Dev 1994;8:1654–1663
7. Rosen ED, Hsu CH, Wang X, et al. C/EBPalpha induces adipogenesis through PPARgamma: a unified pathway. Genes Dev 2002;16:22–26
8. Gregoire FM, Smas CM, Sul HS. Understanding adipocyte differentiation. Physiol Rev 1998;78:783–809
9. Jernås M, Palming J, Sjöholm K, et al. Separation of human adipocytes by size: hypertrophic fat cells display distinct gene expression. FASEB J 2006; 20:1540–1542
10. Maffeis C, Silvagni D, Bonadonna R, Grezzani A, Banzato C, Tatò L. Fat cell size, insulin sensitivity, and inflammation in obese children. J Pediatr 2007; 151:647–652
11. Burton GR, Nagarajan R, Peterson CA, McGehee RE Jr. Microarray analysis of differentiation-specific gene expression during 3T3-L1 adipogenesis. Gene 2004;329:167–185
12. Yeh WC, Cao Z, Classon M, McKnight SL. Cascade regulation of terminal adipocyte differentiation by three members of the C/EBP family of leucine zipper proteins. Genes Dev 1995;9:168–181
13. MacDougald OA, Lane MD. Transcriptional regulation of gene expression during adipocyte differentiation. Annu Rev Biochem 1995;64:345–373
14. Ntambi JM, Young-Cheul K. Adipocyte differentiation and gene expression. J Nutr 2000;130:3122S–3126S
15. Frank D, Mendelsohn CL, Ciccone E, Svensson K, Ohlsson R, Tycko B. A novel pleckstrin homology-related gene family defined by Ipl/Tssc3, TDAG51, and Tih1: tissue-specific expression, chromosomal location, and parental imprinting. Mamm Genome 1999;10:1150–1159
16. Park CG, Lee SY, Kandala G, Lee SY, Choi Y. A novel gene product that couples TCR signaling to Fas(CD95) expression in activation-induced cell death. Immunity 1996;4:583–591
17. Rho J, Gong S, Kim N, Choi Y. TDAG51 is not essential for Fas/CD95 regulation and apoptosis in vivo. Mol Cell Biol 2001;21:8365–8370
18. Gomes I, Xiong W, Miki T, Rosner MR. A proline- and glutamine-rich protein promotes apoptosis in neuronal cells. J Neurochem 1999;73:612–622
19. Hayashida N, Inouye S, Fujimoto M, et al. A novel HSF1-mediated death pathway that is suppressed by heat shock proteins. EMBO J 2006;25:4773–4783
20. Nagai MA, Fregnani JH, Netto MM, Brentani MM, Soares FA. Down-regulation of PHLDA1 gene expression is associated with breast cancer progression. Breast Cancer Res Treat 2007;106:49–56
21. Neef R, Kuske MA, Pröls E, Johnson JP. Identification of the human PHLDA1/TDAG51 gene: down-regulation in metastatic melanoma contributes to apoptosis resistance and growth deregulation. Cancer Res 2002; 62:5920–5929
22. Hossain GS, van Thienen JV, Werstuck GH, et al. TDAG51 is induced by homocysteine, promotes detachment-mediated programmed cell death, and contributes to the cevelopment of atherosclerosis in hyperhomocysteinemia. J Biol Chem 2003;278:30317–30327
23. Basseri S, Lhoták S, Sharma AM, Austin RC. The chemical chaperone 4-phenylbutyrate inhibits adipogenesis by modulating the unfolded protein response. J Lipid Res 2009;50:2486–2501
24. Galic S, Fullerton MD, Schertzer JD, et al. Hematopoietic AMPK β1 reduces mouse adipose tissue macrophage inflammation and insulin resistance in obesity. J Clin Invest 2011;121:4903–4915
25. Sachithanandan N, Fam BC, Fynch S, et al. Liver-specific suppressor of cytokine signaling-3 deletion in mice enhances hepatic insulin sensitivity and lipogenesis resulting in fatty liver and obesity. Hepatology 2010;52: 1632–1642
26. O'Neill HM, Maarbjerg SJ, Crane JD, et al. AMP-activated protein kinase (AMPK) beta1beta2 muscle null mice reveal an essential role for AMPK in maintaining mitochondrial content and glucose uptake during exercise. Proc Natl Acad Sci USA 2011;108:16092–16097
27. Folch J, Lees M, Sloane Stanley GH. A simple method for the isolation and purification of total lipides from animal tissues. J Biol Chem 1957;226:497–509
28. Wei E, Alam M, Sun F, Agellon LB, Vance DE, Lehner R. Apolipoprotein B and triacylglycerol secretion in human triacylglycerol hydrolase transgenic mice. J Lipid Res 2007;48:2597–2606
29. Bligh EG, Dyer WJ. A rapid method of total lipid extraction and purification. Can J Biochem Physiol 1959;37:911–917
30. Fullerton MD, Bakovic M. Complementation of the metabolic defect in CTP:phosphoethanolamine cytidylyltransferase (Pcyt2)-deficient primary hepatocytes. Metabolism 2010;59:1691–1700
31. Dzamko N, van Denderen BJ, Hevener AL, et al. AMPK beta1 deletion reduces appetite, preventing obesity and hepatic insulin resistance. J Biol Chem 2010;285:115–122
32. Ferré P, Foufelle F. Hepatic steatosis: a role for de novo lipogenesis and the transcription factor SREBP-1c. Diabetes Obes Metab 2010;12(Suppl. 2): 83–92
33. Foretz M, Guichard C, Ferré P, Foufelle F. Sterol regulatory element binding protein-1c is a major mediator of insulin action on the hepatic expression of glucokinase and lipogenesis-related genes. Proc Natl Acad Sci USA 1999;96:12737–12742
34. Shimano H, Yahagi N, Amemiya-Kudo M, et al. Sterol regulatory element-binding protein-1 as a key transcription factor for nutritional induction of lipogenic enzyme genes. J Biol Chem 1999;274:35832–35839
35. Furukawa S, Fujita T, Shimabukuro M, et al. Increased oxidative stress in obesity and its impact on metabolic syndrome. J Clin Invest 2004;114: 1752–1761
36. Ravussin E, Smith SR. Increased fat intake, impaired fat oxidation, and failure of fat cell proliferation result in ectopic fat storage, insulin resistance, and type 2 diabetes mellitus. Ann N Y Acad Sci 2002;967:363–378
37. Brown MS, Goldstein JL. Selective versus total insulin resistance: a pathogenic paradox. Cell Metab 2008;7:95–96
38. Bae EJ, Xu J, Oh da Y, et al. Liver-specific p70 S6 kinase depletion protects against hepatic steatosis and systemic insulin resistance. J Biol Chem 2012; 287:18769–18780
39. Sakurai M, Takamura T, Ota T, et al. Liver steatosis, but not fibrosis, is associated with insulin resistance in nonalcoholic fatty liver disease. J Gastroenterol 2007;42:312–317

40. Ferreira DM, Castro RE, Machado MV, et al. Apoptosis and insulin resistance in liver and peripheral tissues of morbidly obese patients is associated with different stages of non-alcoholic fatty liver disease. Diabetologia 2011;54:1788–1798
41. Francque S, Verrijken A, Mertens I, et al. Visceral adiposity and insulin resistance are independent predictors of the presence of non-cirrhotic NAFLD-related portal hypertension. Int J Obes (Lond) 2011;35:270–278
42. Huang J, Jia Y, Fu T, et al. Sustained activation of PPARα by endogenous ligands increases hepatic fatty acid oxidation and prevents obesity in ob/ob mice. FASEB J 2012;26:628–638
43. Zhou QL, Jiang ZY, Mabardy AS, et al. A novel pleckstrin homology domain-containing protein enhances insulin-stimulated Akt phosphorylation and GLUT4 translocation in adipocytes. J Biol Chem 2010;285:27581–27589
44. Toyoshima Y, Karas M, Yakar S, Dupont J, Lee Helman, LeRoith D. TDAG51 mediates the effects of insulin-like growth factor I (IGF-I) on cell survival. J Biol Chem 2004;279:25898–25904
45. Oberst MD, Beberman SJ, Zhao L, Yin JJ, Ward Y, Kelly K. TDAG51 is an ERK signaling target that opposes ERK-mediated HME16C mammary epithelial cell transformation. BMC Cancer 2008;8:189
46. Lemmon MA, Ferguson KM. Signal-dependent membrane targeting by pleckstrin homology (PH) domains. Biochem J 2000;350:1–18
47. Chakraborty A, Koldobskiy MA, Bello NT, et al. Inositol pyrophosphates inhibit Akt signaling, thereby regulating insulin sensitivity and weight gain. Cell 2010;143:897–910
48. Obenauer JC, Cantley LC, Yaffe MB. Scansite 2.0: proteome-wide prediction of cell signaling interactions using short sequence motifs. Nucleic Acids Res 2003;31:3635–3641
49. Kelley LA, Sternberg MJ. Protein structure prediction on the Web: a case study using the Phyre server. Nat Protoc 2009;4:363–371
50. Chan CB, Liu X, Jung DY, et al. Deficiency of phosphoinositide 3-kinase enhancer protects mice from diet-induced obesity and insulin resistance. Diabetes 2010;59:883–893